Electrochemical activity of the polycrystalline cerium oxide films for hydrogen peroxide detection

Electrochemical activity of the polycrystalline cerium oxide films for hydrogen peroxide detection

Julia Kosto[1], Alessandra Zanut[2], Stefano Franchi[3], Yurii Yakovlev[1], Ivan Khalakhan[1], Vladimir Matolin[1], Kevin Charles Prince[3], Giovanni Valenti[2], Francesco Paolucci[2], Nataliya Tsud[1*]

[1] Charles University, Faculty of Mathematics and Physics, Department of Surface and Plasma Science, V Holešovičkách 2, 18000 Prague, Czech Republic

[2] University of Bologna, Department of Chemistry, F. Selmi 2, 40126 Bologna, Italy

[3] Elettra-Sincrotrone Trieste S.C.p.A., in Area Science Park, Strada Statale 14, km 163.5, Basovizza (Trieste), 34149, Italy

[*] Corresponding author: e-mail Nataliya.Tsud@mff.cuni.cz

Abstract

Polycrystalline cerium oxide thin films (15 nm) deposited on a glassy carbon substrate were used as an electrode in a mediator-free, non-enzymatic electrochemical sensor for hydrogen peroxide. The electrode surface was characterized by X-ray photoelectron spectroscopy, resonant photoelectron spectroscopy, scanning electron microscopy and atomic force microscopy. The electrode sensitivity, detection limit and pH range of sensor stability were determined by applying electrochemical techniques: cyclic voltammetry and chronoamperometry. It was found that the sensor reactivity to H_2O_2 is directly related to the presence of electroactive cerium centres of 3+ character on the electrode surface. The Michaelis–Menten mechanism of catalase-like activity of ceria film is suggested as an explanation of the data and discussed. The results confirmed the sensing abilities of technologically

well-accessible nanostructured cerium oxide films for hydrogen peroxide detection without using a mediator, i.e. the enzymatic properties of CeO_2/GC electrode.

Keywords: hydrogen peroxide; cerium oxide; sensor; electrochemistry; resonant photoelectron spectroscopy

1. Introduction

In recent years, development of biological sensors has received much attention in the fields of nanotechnology and materials science. The main effort is directed to the fabrication and characterisation of inorganic materials for novel bioelectrodes with well-defined morphology and physico-chemical properties in reactions with biomolecules and other derivatives of bio recognition events. Electrochemical techniques are well-developed analytical methods widely used for biosensor operation due to their high sensitivity, fast time response, simplicity and accurate determination of specific analytes (cholesterol, glucose, urea, hydrogen peroxide, etc.) [1]. Cerium oxide is among the most promising materials for biological sensing devices. It possesses many bio-related properties like catalytic activity, good biocompatibility, oxygen storage capacity, high isoelectric point, electron transfer capability, etc. [2,3].

Enzymes are often applied as the transduction elements which promote the electrochemical detection of biochemical compounds. The advantages of sensing with enzymes are high efficiency, resolution and specificity, however the catalytic activity of enzymes is unstable as a function of time and sensitive to environmental conditions. Recently, cerium oxide has been actively used for glucose sensor development and improvement. Moumene et al. have reported an enzymatic glucose electrochemical sensor based on pulsed laser deposited nanoceria with glucose oxidase (GOx) physisorbed on an electrode surface [4]. Ansari et al. have fabricated bioelectrodes for glucose detection by deposition of sol-gel derived nanosized CeO_2 films on a gold electrode followed by immobilization of GOx [5]. It demonstrated linearity in the range 50 – 400 mg/dl of glucose. The

same group has reported a cholesterol biosensor constructed by cholesterol oxidase (ChOx) immobilization on sol-gel derived nanostructured cerium oxide film prepared on an indium-tin-oxide coated glass substrate [6]. The electrode's activity has been evaluated as a function of pH, and the data reveal the highest activity at pH 7.0, which corresponds to the natural structure of ChOx. Patil et al. have developed a mediator-less enzymatic glucose biosensor based on a cerium oxide nanorods film electrophoretically deposited onto an indium-tin-oxide coated glass substrate [7]. The electrode demonstrated fast response time and linearity in the range 2 – 26 mM of glucose. Saha et al. have investigated nanoporous ceria thin films deposited onto Pt coated glass plates with immobilized GOx for glucose detection [8]. Results showed a linear range for detection of glucose from 25 to 300 mg/dl and good stability of the bioelectrode.

An alternative approach to enzyme chemistry, based on different inorganic materials possessing enzyme-mimetic properties, is being actively developed and investigated. They are robust to stringent conditions, cheap and have high operational stability, but reveal lower sensitivity and selectivity in comparison with enzymatic electrodes [9]. In the last decades, it was found that nanostructured metal oxides exhibit biocatalytic properties and could be used as artificial enzymes or nanozymes [10,11]. The Pd-CeO_2 platform has been investigated as a biosensing electrode, and electrocatalytic activity toward ascorbic and uric acids, glucose and dopamine was detected [12]. Cerium oxide-based bioelectrodes sensitive to sulfamethoxazole (SMX) in food [13], triglyceride [14], butyrin [15], ochratoxin-A [16] have been investigated. An electrochemical sulfamethoxazole biosensor based on a nano-CeO_2/chitosan composite demonstrated very good selectivity, sensitivity and stability during determination of SMX in egg, milk and honey samples [13].

Hydrogen peroxide is a by-product of several biological processes and can also be a source of many free radicals. It is an essential compound in medicine, biology, the food industry, etc. Thus, it is of great importance to develop and construct simple, cheap, fast, sensitive and precise devices for H_2O_2

detection [17], and several such sensors have been reported [18–25]. Frontera and co-workers have fabricated an electrode for H_2O_2 detection by modifying a planar screen printed carbon electrode by TiO_2/CNTs/Pt nanocomposite dispersed in Nafion solution [18]. It works at a low potential of 0.3 V and can minimize interference with other oxidizable species. The sensor revealed good sensitivity (120 μA mM^{-1} cm^{-2}), linearity from 70 μM to 6 mM and detection limit lower than 5 μM. Jha et al. have proposed a porous CeO_2/ reduced graphene oxide xerogel composite dispersed in Nafion on glassy carbon electrode for the H_2O_2 sensing with linear range from 0.06 μM to 3.0 μM and detection limit 0.03 μM [19]. Yang et al. reported on the H_2O_2 electrocatalytic activity of the CeO_2 nanoparticles onto N-doped reduced oxide graphene nanocomposite films with linear response from 1.8 μM to 0.92 mM and detection limit 1.3 μM [20]. Another example of the electrode for the H_2O_2 detection is reported in Ref. [21], where the Au nanoparticles loaded on the graphene sheets/CeO_2 nanocomposite modified Au electrode were used for H_2O_2 reduction with linear electrocatalytic response in the 1μM – 10 mM range with detection limit 0.26 μM. Mehta et al. developed a 3-terminal amperometric enzyme-free hydrogen peroxide sensor with Au working electrode covered by cerium oxide nanoparticles (NPs) synthesized by a water-in-oil microemulsion technique [22]. The sensor showed linearity in the range from 1 μM to 30 mM H_2O_2. Ansari et al. have reported a bioelectrode for hydrogen peroxide detection based on horseradish peroxidase (HRP) enzyme immobilized on nanosized cerium oxide deposited onto an indium-tin-oxide substrate [23]. The electrode revealed linearity in the range 1 – 170 μM. Neal et al. investigated an enzyme-free cerium oxide NPs-based electrochemical sensor for H_2O_2 detection [24]. The catalytic response to picomolar concentrations of H_2O_2 of NPs with different Ce^{3+}/Ce^{4+} ratio was investigated. The electrode shows an ultra-low detection limit (around 0.1 pM) and linear range from 0.1 pM to 0.1 μM. Nanosized structures with

lower Ce^{3+}/Ce^{4+} ratio were shown to be more electrochemically active, which was in line with results of a catalase assay standard test for evaluation of H_2O_2 neutralization by the same ceria NPs [24].

In this paper we report the application of nanostructured cerium oxide films as a model H_2O_2 sensor. The electrochemical detection of hydrogen peroxide was tested with and without the use of a mediator. The morphology of the polycrystalline cerium oxide thin film prepared by magnetron sputtering in a nonreactive atmosphere on a glassy carbon (GC) substrate was characterised by atomic force microscopy (AFM) and scanning electron microscopy (SEM), while for the stoichiometry and electronic structure evaluation X-ray photoelectron spectroscopy (XPS) and resonant photoelectron spectroscopy (RPES) were applied.

2. Experimental

The 15 nm thick cerium oxide films were prepared by nonreactive magnetron sputtering of a CeO_2 target (99.999%, Kurt J. Lesker), with RF power of 65 W, and argon at a total pressure of 4×10^{-3} mbar as the working gas. The growth rate of cerium oxide on the glassy carbon substrate (Alfa Aesar, 1 mm thick, type 2) at room temperature was 1 nm min^{-1}. The morphology and structure of the CeO_2/GC electrode surface was examined by means of Bruker MultiMode 8 AFM and Tescan Mira 3 SEM microscopes.

The CeO_2/GC electrode characterization by XPS and RPES was conducted at the Materials Science Beamline, Elettra-Sincrotrone Trieste. A detailed description of the beamline end station can be found in Ref. [26]. The Ce 3d core levels were acquired with 1486.6 eV (Al Kα radiation) photon energy and total resolution of 1.00 eV. The valence band (VB) spectra measured at photon energies of 121.4, 124.8 and 115 eV, with total resolution of 0.17 eV, provided resonant spectra of cerium [26]. The emission from Ce 4f states at binding energy about 1.4 eV (photon energy 121.4 eV) and emission from hybridized oxygen-cerium states at about 4.0 eV (photon energy 124.8 eV) relative to the off-

resonance signals (photon energy 115.0 eV) gave resonance enhancements D(Ce^{3+}) and D(Ce^{4+}), respectively, in cations of cerium oxide. The resonance enhancement ratio (RER), i.e. D(Ce^{3+}) to D(Ce^{4+}) signal ratio [26], was analysed and used as a measure of reduction of surface cerium cations (see Results section for details).

Electrochemical characterization of the CeO_2/GC electrode was performed at room temperature using a conventional cell with three electrodes. All potentials were measured versus a Ag/AgCl (3 M KCl) reference electrode purchased from BVT Technologies, and a Pt wire was used as a counter electrode. During the measurements, the working electrode was delimited by an o-ring (6 mm diameter), exposing to the solution an area equal to 0.28 cm^2. The measured current values were expressed as current densities considering the active surface area of the CeO_2/GC electrode. The working solution was phosphate buffered saline (PBS, BioPerformance Certified, heavy metals ≤ 5 ppm) with pH 7 used at concentration of 200 mM for cyclic voltammetry and 10 mM for the chronoamperometry measurements. The ultrapure water (18.2 MΩ.cm from a Millipore MilliQ system, total organic content ≤ 5 ppb) was used to prepare the PBS solutions. Before each experiment the solution was bubbled with nitrogen gas to obtain an oxygen-free environment. Experiments were carried out under nitrogen flow.

Cyclic voltammetry (CV) experiments were performed in the potential range swept between -0.35 V and 0.8 V at a scan rate of 50 mV/s. Furthermore, a set of CV curves was acquired at different pH (from 6 to 8) and at scan rates from 50 to 250 mV/s. The reference CV signals were obtained with bare glassy carbon plate as a working electrode. In measurements with mediator, 2 mM concentration of potassium ferricyanide ($K_3Fe(CN)_6$, Sigma, 99 %) was added to the PBS working solution. Calibration curves were plotted as faradic current versus concentration of hydrogen peroxide.

Prior to chronoamperometry (CA) measurements, two cycles of CV were performed in pure PBS solution to clean the electrode surface and check the functionality of the working electrode. CA experiments were conducted with constant stirring of the solution at potential 0.65 V against the Ag/AgCl electrode. Once a stable current was achieved for the CeO_2/GC electrode in PBS solution, the amperometric response was detected as a function of stepwise additions of H_2O_2 (Sigma, 30 %). The CeO_2/GC electrode was characterized by XPS and RPES after 5 min immersion in the working solution, and after performing CA measurements (about 30 min) in PBS with addition of low (0.05 mM) and high (8 mM) concentrations of H_2O_2. The samples were transferred to UHV under a nitrogen atmosphere (to minimize contamination from the ambient) after the indicated steps in CA.

3. Results

3.1. CeO_2/GC cathode characterization by AFM, SEM, XPS and RPES

The morphology and structure of the CeO_2 film was analysed by AFM and SEM (Fig. 1) and combined with the photoemission analysis of the electronic structure of the oxide surface. The polycrystalline film had a grain size between 10 and 30 nm, measured by both AFM and SEM, in agreement with the published data on similar continuous compact polycrystalline CeO_2 films prepared by magnetron sputtering [27–29]. The surface roughness was about 1.20 nm. The oxide stoichiometry and oxidation state of surface and subsurface Ce cations were examined by measuring the Ce 3d core level and VB spectra. Ce 3d photoelectrons excited by 1486.6 eV photons with kinetic energy about 550 eV provide information about the oxidation state of Ce cations within 5-7 nm of the surface. The shape of the Ce 3d core level (Fig. 2a) corresponds well to a fully oxidized ceria film with a minor contribution of Ce^{3+} centres. The average oxide stoichiometry of $CeO_{1.96}$ was determined by fitting of the Ce 3d spectrum [26]. The analysis of resonant processes in the VB spectra excited by photon energies 121.4 and 124.5 eV (Fig. 2b) provides complementary information about the

oxidation state of cerium cations in the topmost surface layer. The RER value, $D(Ce^{3+})/D(Ce^{4+})$, estimated from RPES was equal to 1.0 confirming the presence of Ce^{3+} cations on the electrode surface. According to Ref. [30], the RER value is 5.5 times the ratio of cerium 3+ to 4+ cations on the surface. Thus, the RER 1.0 can be expressed as 18 Ce^{3+} per 100 Ce^{4+} surface cations (Table 1). The partial reduction of the CeO_2/GC electrode was associated with the polycrystalline structure of the oxide (mainly due to oxygen vacancies on the crystallites surface [28,29]) and with the presence of a small amount of fluorine on the surface of the film (the usual contamination element for commercially available cerium or cerium oxide). As the ceria film was stored in air and analysed in UHV without cleaning, the adventitious carbon and fluorine were detected on the surface roughly in the ratio 1.7 to 1 (Table 1). The C 1s core level is characterized by a major peak at 285.0 eV due to atomic carbon and a small component at 289.0 eV assigned to oxygenated hydrocarbons overlapping the Ce 4s signal. We do not expect a significant carbon signal from the underlying GC substrate as the oxide film is 15 nm thick. We believe that the F 1s signal at 684.5 eV originates rather from the surface than from the bulk of the CeO_2 film because it vanished almost completely in the course of the electrochemical experiment and the shape of the Ce 3d core level (Fig. 3) does not show traces of the formation of CeO_xF_y mixed oxide [31]. The O 1s core level (not shown here) is dominated by one peak at 529.6 eV assigned to the lattice oxygen from cerium oxide with a small shoulder at 531.5 eV due to adsorbed oxygenated hydrocarbons and hydroxyl groups. The immersion in PBS further reduces the surface, accompanied by adsorption of phosphorus, sodium, potassium and chlorine. The attenuation of the Ce 3d core level expressed as a Ce 3d area relative to the signal of the clean oxide (see Table 1) is a measure of thickness of the P, Na, K and Cl adlayer formed as a result of the working electrode interaction with PBS in the course of the electrochemical experiments.

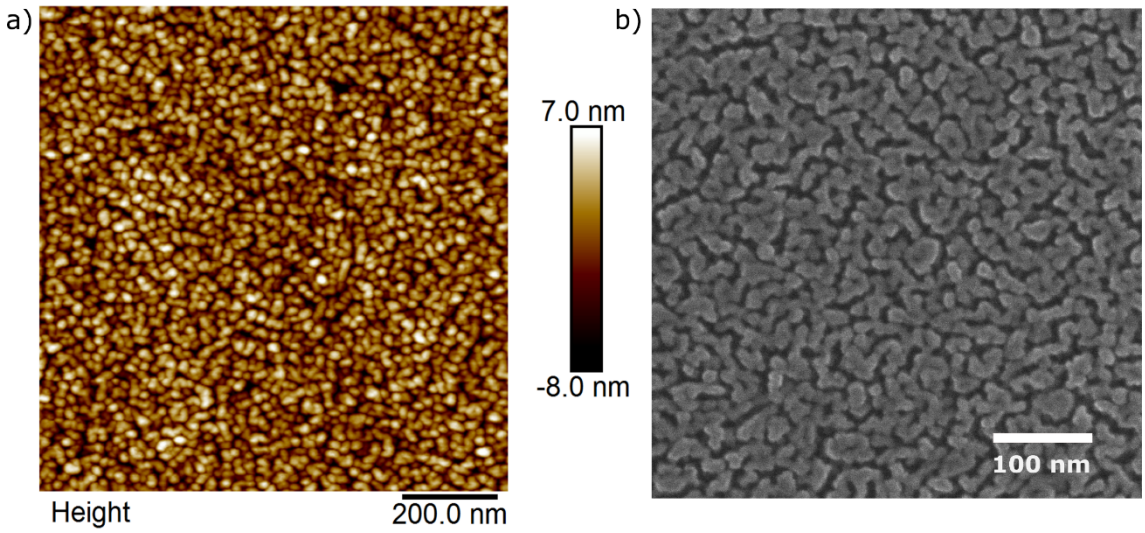

Fig.1. a) AFM and b) SEM images of polycrystalline CeO_2 film deposited on the glassy carbon electrode.

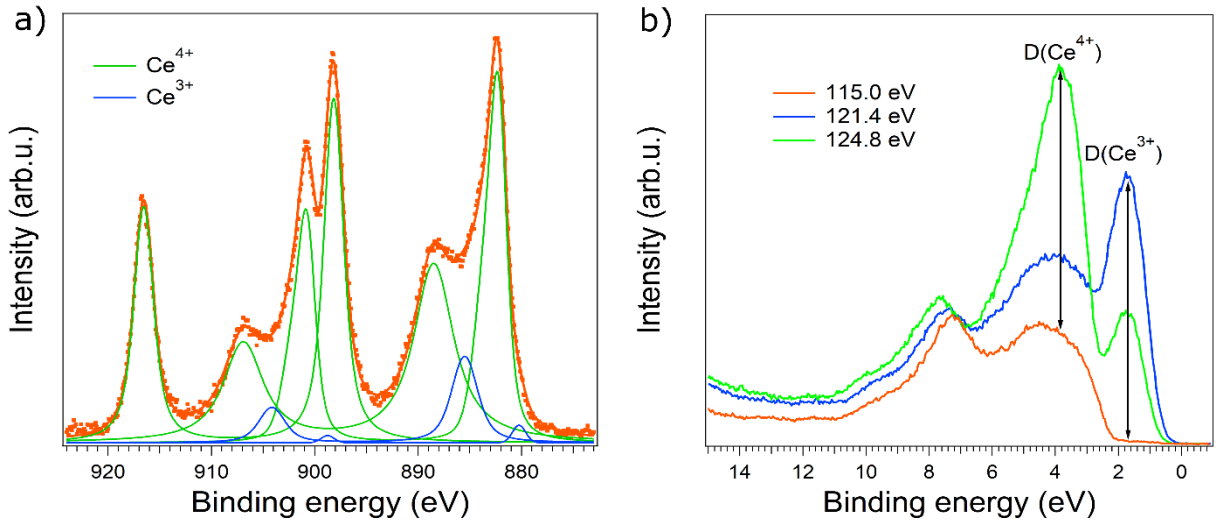

Fig. 2. a) XPS Ce 3d core level and b) RPES valence spectra of the CeO_2/GC electrode.

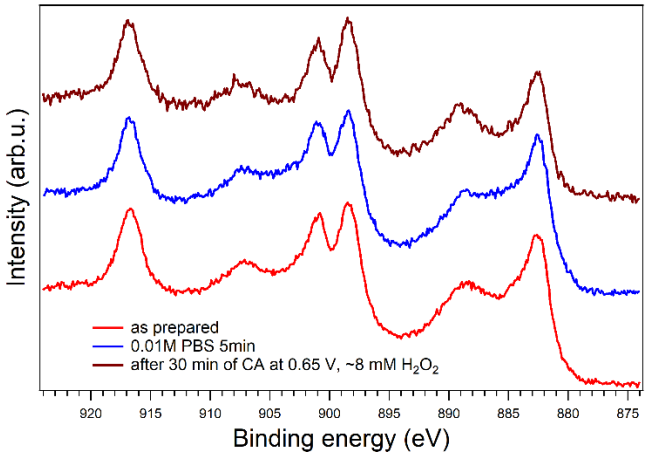

Fig. 3. Ce 3d spectra normalized to the maxima for differently treated CeO_2/GC electrodes.

Table 1. The RER values, the ratio of Ce^{3+} and Ce^{4+} cations on the surface, average cerium oxide film stoichiometry together with the relative Ce 3d area and the ratio of normalized (C 1s+Ce 4s) to F 1s XPS signals for the different experimental steps.

CeO_2/GC	VB (RPES) RER	$n(Ce^{3+}) / n(Ce^{4+})$	Ce 3d (XPS), Relative area	I(C 1s+Ce 4s) /I(F 1s)
as prepared	1.0	18 / 100	$CeO_{1.96}$, 1.0	1.7 / 1.0
10 mM PBS	1.7	31 / 100	$CeO_{1.94}$, 0.86	4.2 / 1.0
CA at 0.65 V in 10 mM PBS + 0.05 mM H_2O_2	0.4	7 / 100	$CeO_{1.97}$, 0.68	6.0 / 1.0
CA at 0.65 V in 10 mM PBS + 8 mM H_2O_2	0.2	3.5 / 100	$CeO_{1.97}$, 0.24	20.0 / 1.0

3.2. H_2O_2 sensing by CeO_2/GC nanostructured cathode - cyclic voltammetry

The cyclic voltammetry curves of the CeO_2/GC working electrode in 200 mM PBS with and without mediator are shown in Figure 4 in comparison with data for bare GC. We observe that the CeO_2/GC electrode has a good conductibility and a larger electro active area compared to bare GC. The total

surface area of the electrode has an important effect on the reaction rate for heterogeneous catalysts and it is bigger in the case of polycrystalline ceria film compared to a GC electrode giving higher CV current. Thus, the presence of the cerium oxide promotes the electron transfer without the use of mediator. The CV curve of the CeO_2/GC electrode in the presence of the mediator indicates the further enhancement of the electron transfer between working and counter electrodes. A difference of 270 mV between the oxidation and reduction peaks characteristic for mediator on CeO_2/GC, close to the value of 320 mV on GC (Fig. 4), confirms good transducer properties of the ceria electrode. The kinetics of the electrochemical reactions on the CeO_2/GC electrode was shown to be surface-controlled and stable in the pH range from 6 to 8 (for details see Fig. S1 of Supplementary Materials). To explore the response of the CeO_2/GC electrode to an increasing concentration of hydrogen peroxide, cyclic voltammetry measurements were performed in 200 mM PBS at pH 7 with and without mediator (Fig. 5). The 2 mM $K_3Fe(CN)_6$ redox mediator was used with the aim to facilitate the electron transfer processes in the working solution. The H_2O_2 was introduced stepwise from a minimum concentration of 5 μM to a maximum total concentration of 8388 μM. A gradual increase in the anodic current upon the addition of H_2O_2 was observed without clear peaks in the case of the working solution without mediator. For the oxidation region, the calibration curves were plotted at potential 0.65 and 0.80 V and are shown in the inset of Figure 5a. Both curves increase with H_2O_2 concentration. Notice that CeO_2/GC shows a remarkable onset potential of about 0.55-0.60 V for the H_2O_2 oxidation, which is comparable with the most active systems for H_2O_2 oxidation reported to date [32]. In order to study the catalytic mechanism of hydrogen peroxide oxidation on the surface of cerium oxide, we repeated the experiment with different H_2O_2 concentration in the presence of a redox mediator (Fig. 5b). In line with previous results the anodic currents, measured at 0.65 and 0.8 V, increases systematically with increase of H_2O_2 concentration, and the maximum current values reached at 0.65 and 0.8 V are similar to the case of working solution without mediator. Furthermore,

the current increase was only negligible in the case of pristine GC and thus it was linked to the activity of the ceria cations on the electrode surface. Additionally, the reversible oxidation at $E_{1/2}$ of 0.2 V corresponds to H_2O_2 reaction at the mediator centres.

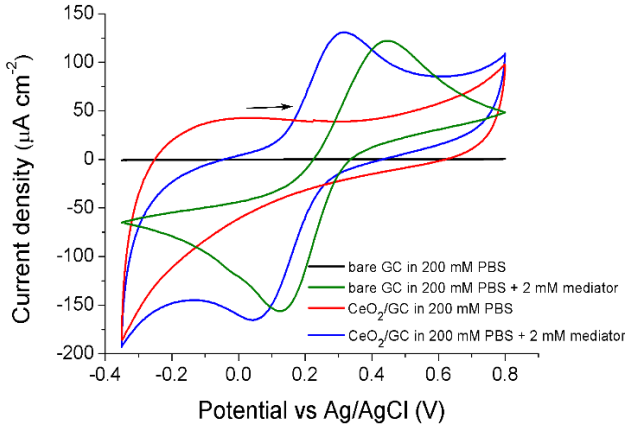

Fig. 4. The CV curves of CeO_2/GC and GC electrodes in 200 mM PBS with and without 2 mM $K_3Fe(CN)_6$.

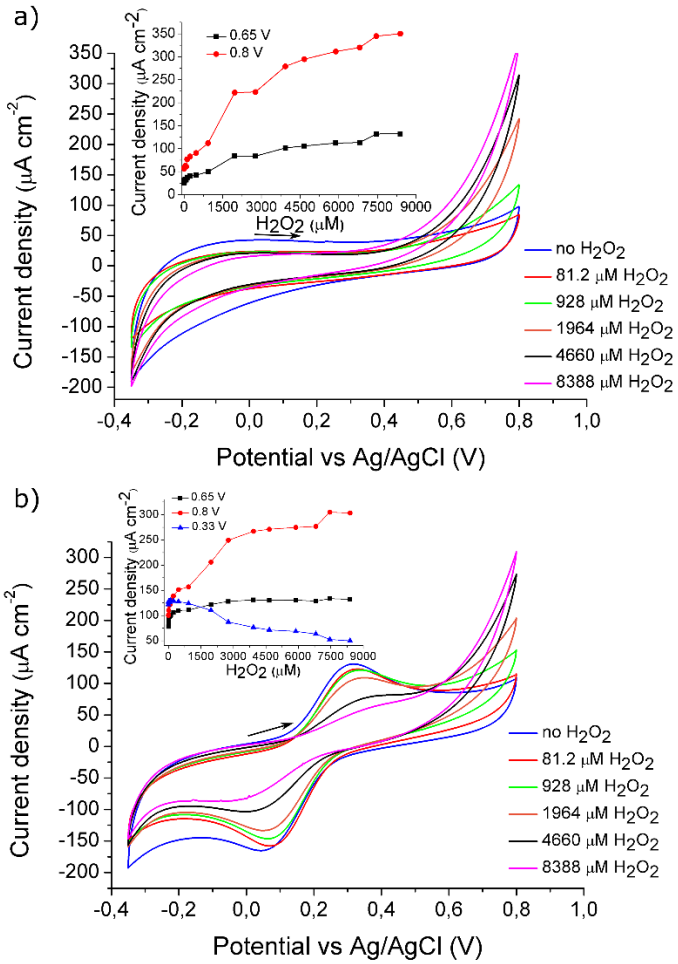

Fig. 5. Cyclic voltammogram of a CeO_2/GC electrode as a function of H_2O_2 concentration without (a) and with 2 mM $K_3Fe(CN)_6$ (b). Insets: calibration curves plotted at potentials 0.65 V and 0.8 V (a), and at 0.33 V, 0.65 V and 0.8 V (b). The CV was measured in 200 mM PBS at pH 7 at a scan rate 50 mVs^{-1}.

The magnitude of the anodic peak at 0.33 V decreases with increase of H_2O_2 concentration (see the calibration curve at 0.33 V in the inset of Fig. 5b). This is likely due to the competition between H_2O_2 and the redox mediator molecules in the interaction with the active sites on the electrode surface which is not in favour of the latter. The CV performance of the CeO_2/GC electrode in the presence of the mediator confirms the important role of oxygen vacancies on the CeO_2/GC electrode surface in

the reaction with H_2O_2. This statement is also supported by chronoamperometry results presented below.

3.3. H_2O_2 sensing by CeO_2/GC nanostructured cathode - chronoamperometry and RPES

The CeO_2/GC electrode activity was characterised by chronoamperometry performed applying a constant potential of 0.65 V versus Ag/AgCl with increasing concentration of hydrogen peroxide (Fig. 6a). In this case 10 mM PBS working solution at pH 7 was used in order to reduce the formation of cerium phosphate, which might passivate the electrode surface and hinder the H_2O_2 oxidation on the ceria active centres [33]. The dependence of the stabilized current value at each step on the H_2O_2 concentration, i.e. the calibration curve (see the inset in Fig. 6a), shows the high sensitivity of the CeO_2/GC electrode to the low concentration of hydrogen peroxide. The shape of the calibration curve is typical for the enzymatic reactions, showing a Michaelis–Menten mechanism, which confirms the enzymatic-like activity of the working electrode [34]. The region where the current density increases linearly with H_2O_2 (0.005 – 0.460 mM) defines a first-order reaction of hydrogen peroxide on the CeO_2/GC electrode with sensitivity factor of ~ 0.7 $\mu A\ \mu M^{-1}\ cm^{-2}$. Then, the current gradually reaches a plateau (starting from 4.5 mM) indicating the completion of the reaction between the active sites of the electrode and H_2O_2, i.e. a further increase in the H_2O_2 concentration does not change the reaction speed any more, and therefore constitutes a zero-order reaction mechanism. The Michaelis-Menten constant (*K*m) was estimated from the Lineweaver–Burk plot. It represents the catalytic efficiency of an enzyme or enzyme-mimetic material in conversion of H_2O_2 into products. Thus, for hydrogen peroxide, molecules or biomaterials with lower *K*m are more efficient, i.e. lower concentration of H_2O_2 is needed to obtain a maximum activity of an electrode. The measured values are presented in Table 2 and compared with recently published results of other nanozymes and HRP.

The top of the VB spectra of the CeO_2/GC electrode after chronoamperometry at low (~50 μM) and high (~8 mM) H_2O_2 concentrations is shown in Figure 6b, corresponding to the linear 0.05 – 0.46 mM and saturation 4.5 – 8.4 mM region of the calibration curve, respectively. The corresponding RER values and the estimated ratio of surface Ce^{3+} to Ce^{4+} cations are shown in Table 1. The change of the D(Ce^{3+}) peak intensity after CA experiments evidences the involvement of the Ce^{3+} cations in the H_2O_2 oxidation on the electrode surface. Specifically, low H_2O_2 concentration caused a strong decrease of the Ce^{3+} intensity, while this peak vanished completely when saturation is reached. Thus, the plateau in amperometric response was attributed to electrode reoxidation, i.e. the substantial decrease in concentration of the Ce^{3+} cations and oxygen vacancies on the surface of the working electrode. The average cerium oxide film stoichiometry remains unchanged after CA, while the intensity of the Ce 3d core level is strongly reduced for the H_2O_2 saturated region where the Ce^{3+} concentration is minimal (see Table 1). We can conclude that the less reactive the surface becomes, the more adsorbed species are formed on the surface in a given time. The Ce 3d core level behaviour, i.e. increased intensity of the valley at 886 eV (see Fig. 3), confirms the reduction of the electrode within a depth of 7 nm (defined by the Ce 3d photoelectron kinetic energy of about 550 eV) provide information after PBS treatment, and then partial reoxidation after reaction with H_2O_2.

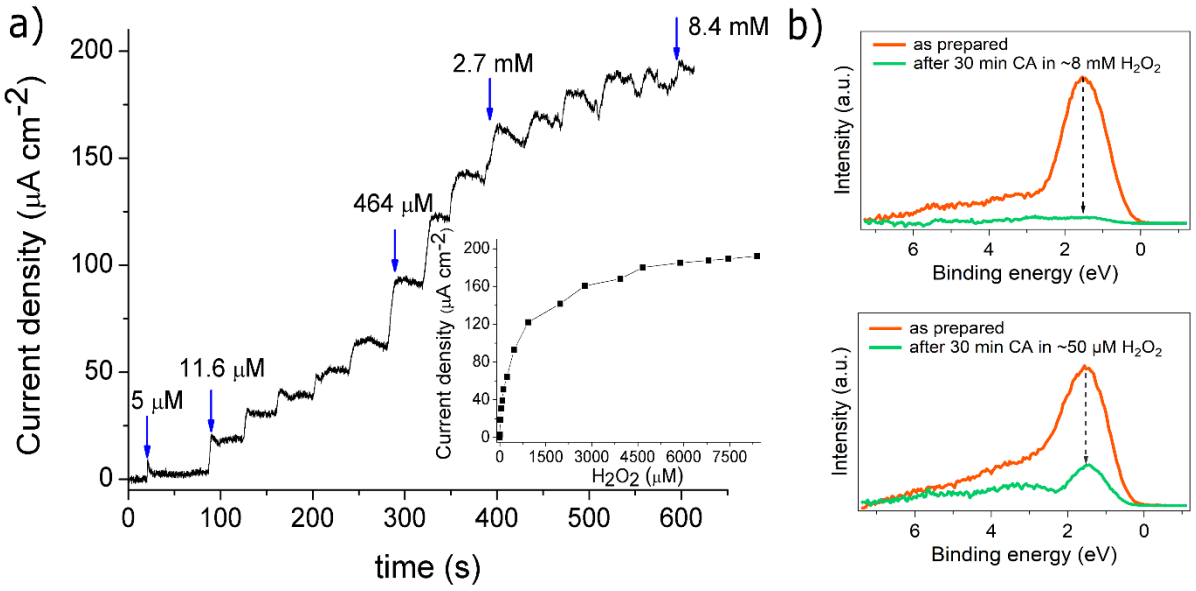

Fig. 6. a) Amperometric response of the CeO_2/GC electrode at 0.65 V vs Ag/AgCl with stepwise H_2O_2 concentration increasing from 0 to 8 mM, in 10 mM PBS. The inset shows the dependence of the current density versus H_2O_2 concentration; b) Change of the D(Ce^{3+}) resonance VB peak measured by RPES of the as-prepared (red) films and after chronoamperometry (green) at high (~8 mM) and low (~50 μM) H_2O_2 concentrations.

Table 2. Comparison of the Michaelis-Menten constant (*K*m) for hydrogen peroxide between CeO_2/GC, other nanozymes and HRP.

Catalyst	*K*m, mM	Reference
RF CeO_2/GC	1.02	This paper
CeO_2 NPs	64.60	[28]
CeO_2/NT-TiO_2	0.04	[29]
H_2TCPP-CeO_2 NPs	0.254	[30]
CeO_2 NPs	0.278	[30]
$LaNiO_3$	90.05	[31]
Au/CeO_2-chitosan composite film	1.93	[32]
Fe_3O_4	154	[33]
HRP	3.70	[33,34]

4. Discussion

The CeO_2/GC electrode acts as a catalyst in the oxidation of H_2O_2 under applied voltage. To understand the enzymatic-like activity of ceria it is important to characterise the active centres on the electrode surface and reaction mechanism of the H_2O_2 oxidation. According to the published data on CeO_2 NPs, the active centres responsible for the anti-oxidation behaviour are proposed to be mainly determined by surface Ce sites that can coordinate the oxygen species [24,35]. Apparently for the CeO_2/GC electrode the possible active centres, i.e. the sites where the reaction occurs, are Ce^{4+} and Ce^{3+} cations and oxygen vacancies. In our experiments, the as-prepared CeO_2 electrode surface is partially reduced, i.e. we have a polycrystalline ceria film with a mixture of Ce^{4+} and Ce^{3+} cations on the surface. The RPES analysis shows that immersion in PBS and CV cycling further reduce the electrode surface. Once the hydrogen peroxide is introduced into the working solution under applied

voltage, ceria acts as a nanozyme - adsorbing H_2O_2 promotes the electrochemical reaction by sharing its electrons. We assume that the oxidation mechanism of H_2O_2 on the CeO_2/GC electrode can be expressed by the reaction [36]:

$$H_2O_2 = O_2 + 2H^+ + 2e^-, \quad (1)$$

Here, apart from the electrochemical current increase connected with the formation of electrons ($2e^-$), a pH change to lower values is expected. As the detected pH change was minor and in the opposite direction, we conclude we have observed more complex behaviour, such as a catalase-like activity of cerium oxide [3,33,37–39]. The mechanism of the reaction might be expressed by the equations (2) and (3), summarized by the net reaction (4):

$$2Ce^{3+} + H_2O_2 \Rightarrow Ce^{4+} + Ce^{4+}\text{-}O_{ads} + H_2O + 2e^- \quad (2)$$

$$Ce^{4+} + Ce^{4+}\text{-}O_{ads} + H_2O_2 \Rightarrow 2Ce^{3+} + H_2O + O_2 + 2e^- \quad (3)$$

$$2H_2O_2 \Rightarrow O_2 + 2H_2O, \quad (4)$$

where $Ce^{4+}\text{-}O_{ads}$ denotes adsorbed oxygen species, which transforms the Ce^{3+} cations with nearby vacancy into Ce^{4+} sites. The produced electrons form the current increase in the electrochemical data, and they are accommodated by cerium cations. As a result, we obtained a solution enriched by O_2 (note that experiments were carried out in an oxygen free solution). This oxygen may react with vacancies and be a primary reason of the ceria surface deactivation in its reaction with H_2O_2. The formation of free radicals is unlikely but we do not have direct proof, as in the published data [39]. Thus, the electrode surface is oxidizing during the electrochemical reaction of H_2O_2 on the surface of cerium oxide. The reaction stops when no Ce^{3+} centres are available for the reaction. Moreover, immersion in the working solution and CV cycling reduces the electrode surface and offers a way to regenerate the Ce^{3+} active centres. The schematic illustration of the electrochemical reaction of H_2O_2 on the CeO_2/GC electrode surface is shown in Figure 7. The suggested reaction mechanism agrees

well with the phase diagram of hydrogen peroxide decomposition in water [36], where the region of pH 7 and voltage 0.65 V corresponds to a double instability of H_2O_2: reduction to H_2O and oxidation to O_2.

The typical Michaelis-Menten curve and *K*m parameter of 1.02 mM for the oxidation of H_2O_2 on CeO_2/GC indicate increased affinity of H_2O_2 for the surface of cerium oxide as compared (see Table 2) to CeO_2 NPs (64.60 mM) [40], Au/CeO_2-chitosan composite films (1.93 mM) [41] and HRP enzyme (3.70 mM) [42,43], underlining the advantage of polycrystalline surface morphology of the working electrode. The absence of a H_2O_2 oxidation peak suggests that the CeO_2 matrix is acting as a good electron acceptor and confirms the direct electron exchange via the ceria surface. As suggested in previously published works [44,45], we link it to the presence of the Ce^{3+} cations on the electrode surface. We conclude that the hydrogen peroxide reaction on the ceria electrode is managed via efficient adsorption of oxygenated species on the Ce^{3+} cations or oxygen defects and direct electron transfer through Ce^{3+} and Ce^{4+} redox centres. The observed linear response as a function of H_2O_2 concentration indicates that the CeO_2/GC electrode can be efficiently used for H_2O_2 detection over the concentration range 0.005 – 0.460 mM.

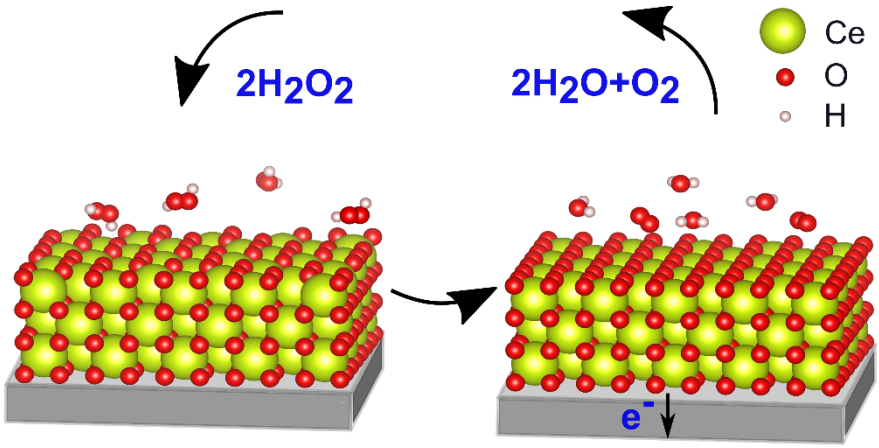

Fig. 7. Schematic illustration of the electrochemical reaction of H_2O_2 on the CeO_2/GC electrode surface.

Nanostructured cerium oxide is widely used as an electrode material in electrochemistry, which is usually prepared by chemical methods, for instance by deposition from solution [7,12–16,19,21,23,24,40,44]. The ceria electrode was shown to provide an enhanced electron communication between the working solution and the cathode during electrochemical deactivation of H_2O_2, independently of the absence or presence of enzymes/mediators. In agreement with our work, the published data report the oxidation of the CeO_2 particles on the electrode surface in the course of the H_2O_2 electrochemical reaction, often confirmed by red shift of UV-vis features. Our findings are in line with work of Pirmohamed et al. [35]. They confirmed the catalase mimetic properties of nanoceria and affirmed that this catalytic reaction is not equivalent for all nanoceria preparations correlating with the presence of cerium cations in the 3+ state. The authors closely linked the change in Ce^{3+} cation concentration at the NPs surface with their improved catalytic activity versus H_2O_2. It was even shown that immersion in PBS led to an improved catalase mimetic activity of cerium oxide NPs [35]. The only significant difference with respect to our results is the conclusion regarding oxidation of NPs after immersion in PBS, deduced from the red shift of UV-vis features, while we demonstrated the surface reduction of ceria films. Whether this discrepancy relates to the cerium oxide morphology (NPs versus thin films) or to different techniques of analysis (UV-vis versus RPES) it is not clear. Another closely related work is Ref. [24], where the working electrode with CeO_2 NPs was tested as an enzyme-free H_2O_2 sensor in the 0.5 pM – 5.0 mM range. The higher EC signals were generated on the electrode with the lowest Ce^{3+}/Ce^{4+} ratio in agreement with our results. The absolute Ce^{3+}/Ce^{4+} values cannot be directly compared because of difference in the applied surface characterisation techniques. The linearity range 5 – 460 μM for our CeO_2/GC electrode is

higher compared with 0.1 pM – 0.1 μM for the CeO_2 NPs based electrode from Ref. [24], most likely due to insufficient experimental cleanliness in the present study. The recent work of Li et al. [46] is an example of the application of ceria NPs deposited by magnetron sputtering on TiO_2 used for tissue engineering and regenerative medicine. In general, introduction of an implant into the body initiates an inflammatory cascade due to cell and tissue damage, which is closely related to a local increase of reactive oxygen species formation, such as superoxide and hydrogen peroxide. This work confirmed the importance of the Ce^{3+}/Ce^{4+} **ratio for the** new bone formation adjacent to the inorganic implant on the base of cerium oxide. Specifically, the manipulation of valence states of ceria NPs appeared to provide an effective modulation of the balance of anti-inflammatory and proinflammatory processes and create an anti-inflammatory microenvironment [46]. Summarizing, the morphologically different ceria electrode, i.e. the compact polycrystalline CeO_2 film in the present work is suitable as an electrode for the electrochemical detection of hydrogen peroxide. The CeO_2/GC electrode showed catalytic activity versus H_2O_2, due to available oxygen vacancies and high specific area. Thus, cerium oxide in the form of thin films provides the outstanding properties of ceria NPs, offering a compact polycrystalline electrode material for sensing devices.

5. Conclusions

Polycrystalline cerium oxide films are proposed for electrochemical detection of hydrogen peroxide. The electrode was characterized by photoelectron spectroscopy and microscopy. The CeO_2/GC electrode surface was formed by compact polycrystalline cerium oxide with the cerium cations in both 4+ and 3+ states. The sensor was tested in PBS solution at 25 °C in the H_2O_2 concentration range from 5 μM to 8 mM. The CeO_2/GC exhibited high sensitivity and linear response in the low H_2O_2 concentration range. The sensor sensitivity was estimated to be 0.7 $\mu A\ \mu M^{-1}\ cm^{-2}$. The detection limit

is below 5 μM of H_2O_2. We conclude that H_2O_2 molecules are bound to the oxygen vacancies in the vicinity of Ce^{3+} cations on the surface of the electrode. Thus, ceria absorbs H_2O_2 and coordinates the electrochemical reaction by sharing its electrons. The enzymatic properties of the polycrystalline CeO_2/GC electrode were confirmed. The results bring important knowledge and direct proof of the Ce^{3+} cations role in H_2O_2 sensing by cerium oxide electrodes.

Acknowledgement

We gratefully acknowledge the assistance of our colleagues at Elettra for providing good quality synchrotron light. CERIC-ERIC consortium, Grant Agency of Charles University (GAUK project No. 1054217) and Czech Ministry of Education (LM2015057) are acknowledged for financial support. AZ, GV and FP thank the University of Bologna, Italian Ministero dell'Istruzione, Universita e Ricerca (MIUR-project PRIN 2018), FARB and Fondazione CARISBO.

Supplementary Materials: The CV curves for the CeO_2/GC electrode as function of scan rates and different pH.

References

[1] Y.-B. Hahn, R. Ahmad, N. Tripathy, Chemical and biological sensors based on metal oxide nanostructures., Chem. Commun. (Camb). 48 (2012) 10369–85. doi:10.1039/c2cc34706g.

[2] C. Xu, X. Qu, Cerium oxide nanoparticle: a remarkably versatile rare earth nanomaterial for biological applications, NPG ASIA Mater. 6 (2014) e90-16. doi:10.1038/am.2013.88.

[3] I. Celardo, J.Z. Pedersen, E. Traversa, L. Ghibelli, Pharmacological potential of cerium oxide nanoparticles, Nanoscale. 3 (2011) 1411–1420. doi:10.1039/c0nr00875c.

[4] M. Moumene, A. Tabet-Aoul, M. Gougis, D. Rochefort, M. Mohamedi, Laser pulse

deposited nanosized ceria for direct electron transfer of glucose oxidase, Int. J. Electrochem. Sci. 9 (2014) 176–184.

[5] A. a. Ansari, P.R. Solanki, B.D. Malhotra, Sol-gel derived nanostructured cerium oxide film for glucose sensor, Appl. Phys. Lett. 92 (2008) 263901. doi:10.1063/1.2953686.

[6] A.A. Ansari, A. Kaushik, P.R. Solanki, B.D. Malhotra, Sol-gel derived nanoporous cerium oxide film for application to cholesterol biosensor, Electrochem. Commun. 10 (2008) 1246–1249. doi:10.1016/j.elecom.2008.06.003.

[7] D. Patil, N.Q. Dung, H. Jung, S.Y. Ahn, D.M. Jang, D. Kim, Enzymatic glucose biosensor based on CeO2 nanorods synthesized by non-isothermal precipitation., Biosens. Bioelectron. 31 (2012) 176–81. doi:10.1016/j.bios.2011.10.013.

[8] S. Saha, S.K. Arya, S.P. Singh, K. Sreenivas, B.D. Malhotra, V. Gupta, Nanoporous cerium oxide thin film for glucose biosensor., Biosens. Bioelectron. 24 (2009) 2040–5. doi:10.1016/j.bios.2008.10.032.

[9] P.R. Solanki, A. Kaushik, V. V Agrawal, B.D. Malhotra, Nanostructured metal oxide-based biosensors, NPG ASIA Mater. 3 (2011) 17–24. doi:10.1038/asiamat.2010.137.

[10] Y. Lin, J. Ren, X. Qu, Catalytically active nanomaterials: a promising candidate for artificial enzymes, Acc. Chem. Res. 47 (2014) 1097–1105. doi:10.1021/ar400250z.

[11] X. Wang, Y. Hu, H. Wei, Nanozymes in bionanotechnology: from sensing to therapeutics and beyond, Inorg. Chem. Front. 3 (2016) 41–60. doi:10.1039/C5QI00240K.

[12] F. Qu, H. Sun, S. Zhang, J. You, M. Yang, Electrochemical sensing platform based on palladium modified ceria nanoparticles, Electrochim. Acta. 61 (2012) 173–178. doi:10.1016/j.electacta.2011.11.113.

[13] M. Cai, L. Zhu, Y. Ding, J. Wang, J. Li, X. Du, Determination of sulfamethoxazole in foods based on CeO 2/ chitosan nanocomposite-modified electrodes, Mater. Sci. Eng. C. 32 (2012)

2623–2627. doi:10.1016/j.msec.2012.08.017.

[14] P.R. Solanki, C. Dhand, A. Kaushik, A. a. Ansari, K.N. Sood, B.D. Malhotra, Nanostructured cerium oxide film for triglyceride sensor, Sensors Actuators B Chem. 141 (2009) 551–556. doi:10.1016/j.snb.2009.05.034.

[15] S. Panky, K. Thandavan, D. Sivalingam, S. Sethuraman, U.M. Krishnan, B.G. Jeyaprakash, J.B.B. Rayappan, Lipase immobilized on nanostructured cerium oxide thin film coated on transparent conducting oxide electrode for butyrin sensing, Mater. Chem. Phys. 137 (2013) 892–897. doi:10.1016/j.matchemphys.2012.10.031.

[16] A. Kaushik, P.R. Solanki, A.A. Ansari, S. Ahmad, B.D. Malhotra, A nanostructured cerium oxide film-based immunosensor for mycotoxin detection, Nanotechnology. 20 (2009) 055105–055112. doi:10.1088/0957-4484/20/5/055105.

[17] M. Malferrari, A. Ghelli, F. Roggiani, G. Valenti, F. Paolucci, M. Rugolo, S. Rapino, Reactive Oxygen Species Produced by Mutated Mitochondrial Respiratory Chain of Entire Cells Monitored with Modified Microelectrodes, ChemElectroChem. 0 (2018). doi:10.1002/celc.201801424.

[18] P. Frontera, A. Malara, S. Stelitano, S.G. Leonardi, A. Bonavita, E. Fazio, P. Antonucci, G. Neri, F. Neri, S. Santangelo, Characterisation and H2O2 sensing properties of TiO2-CNTs/Pt electro-catalysts, Mater. Chem. Phys. 170 (2016) 129–137. doi:http://dx.doi.org/10.1016/j.matchemphys.2015.12.030.

[19] S.K. Jha, C.N. Kumar, R.P. Raj, N.S. Jha, S. Mohan, Synthesis of 3D porous CeO2/reduced graphene oxide xerogel composite and low level detection of H2O2, Electrochim. Acta. 120 (2014) 308–313. doi:https://doi.org/10.1016/j.electacta.2013.12.051.

[20] S. Yang, G. Li, G. Wang, L. Liu, D. Wang, L. Qu, Synthesis of highly dispersed CeO2 nanoparticles on N-doped reduced oxide graphene and their electrocatalytic activity toward

H2O2, J. Alloys Compd. 688 (2016) 910–916. doi:https://doi.org/10.1016/j.jallcom.2016.07.113.

[21] X. Yang, Y. Ouyang, F. Wu, Y. Hu, Y. Ji, Z. Wu, Size controllable preparation of gold nanoparticles loading on graphene sheets@cerium oxide nanocomposites modified gold electrode for nonenzymatic hydrogen peroxide detection, Sensors Actuators B Chem. 238 (2017) 40–47. doi:https://doi.org/10.1016/j.snb.2016.07.016.

[22] A. Mehta, S. Patil, H. Bang, H.J. Cho, S. Seal, A novel multivalent nanomaterial based hydrogen peroxide sensor, Sensors Actuators A Phys. 134 (2007) 146–151. doi:https://doi.org/10.1016/j.sna.2006.05.028.

[23] A.A. Ansari, P.R. Solanki, B.D. Malhotra, Hydrogen peroxide sensor based on horseradish peroxidase immobilized nanostructured cerium oxide film, J. Biotechnol. 142 (2009) 179–184. doi:https://doi.org/10.1016/j.jbiotec.2009.04.005.

[24] C.J. Neal, A. Gupta, S. Barkam, S. Saraf, S. Das, H.J. Cho, S. Seal, Picomolar Detection of Hydrogen Peroxide using Enzyme-free Inorganic Nanoparticle-based Sensor, Sci. Rep. 7 (2017) 1324. doi:10.1038/s41598-017-01356-5.

[25] H.-H. Zeng, W.-B. Qiu, L. Zhang, R.-P. Liang, J.-D. Qiu, Lanthanide Coordination Polymer Nanoparticles as an Excellent Artificial Peroxidase for Hydrogen Peroxide Detection, Anal. Chem. 88 (2016) 6342–6348. doi:10.1021/acs.analchem.6b00630.

[26] S. Bercha, K. Beranová, R.G. Acres, M. Vorokhta, M. Dubau, I. Matolínová, T. Skála, K.C. Prince, V. Matolín, N. Tsud, Thermally Controlled Bonding of Adenine to Cerium Oxide: Effect of Substrate Stoichiometry, Morphology, Composition, and Molecular Deposition Technique, J. Phys. Chem. C. 121 (2017) 25118–25131. doi:10.1021/acs.jpcc.7b06925.

[27] M. Dubau, J. Lavková, I. Khalakhan, S. Haviar, V. Potin, V. Matolín, I. Matolínová, Preparation of magnetron sputtered thin cerium oxide films with a large surface on silicon

substrates using carbonaceous interlayers., ACS Appl. Mater. Interfaces. 6 (2014) 1213–8. doi:10.1021/am4049546.

[28] V. Potin, J. Lavkova, S. Bourgeois, M. Dubau, I. Matolinova, V. Matolin, Structural and Chemical Characterization of Cerium Oxide Thin Layers Grown on Silicon Substrate, Mater. Today Proc. 2 (2015) 101–107. doi:http://dx.doi.org/10.1016/j.matpr.2015.04.014.

[29] J. Lavkova, I. Khalakhan, M. Chundak, M. Vorokhta, V. Potin, V. Matolin, I. Matolinova, Growth and composition of nanostructured and nanoporous cerium oxide thin films on a graphite foil, Nanoscale. 7 (2015) 4038–4047. doi:10.1039/C4NR06550F.

[30] Y. Lykhach, S.M. Kozlov, T. Skala, A. Tovt, V. Stetsovych, N. Tsud, F. Dvorak, V. Johanek, A. Neitzel, J. Myslivecek, S. Fabris, V. Matolin, K.M. Neyman, J. Libuda, Counting electrons on supported nanoparticles, Nat Mater. 15 (2016) 284–288. http://dx.doi.org/10.1038/nmat4500.

[31] M. Kettner, K. Ševčíková, P. Homola, V. Matolín, V. Nehasil, Influence of the Ce–F interaction on cerium photoelectron spectra in CeOXFY layers, Chem. Phys. Lett. 639 (2015) 126–130. doi:https://doi.org/10.1016/j.cplett.2015.09.018.

[32] Y. Li, C. Sella, F. Lemaître, M. Guille Collignon, L. Thouin, C. Amatore, Highly Sensitive Platinum-Black Coated Platinum Electrodes for Electrochemical Detection of Hydrogen Peroxide and Nitrite in Microchannel, Electroanalysis. 25 (2013) 895–902. doi:10.1002/elan.201200456.

[33] R. Singh, S. Singh, Role of phosphate on stability and catalase mimetic activity of cerium oxide nanoparticles., Colloids Surf. B. Biointerfaces. 132 (2015) 78–84. doi:10.1016/j.colsurfb.2015.05.005.

[34] A. Juzgado, A. Soldà, A. Ostric, A. Criado, G. Valenti, S. Rapino, G. Conti, G. Fracasso, F. Paolucci, M. Prato, Highly sensitive electrochemiluminescence detection of a prostate cancer

biomarker, J. Mater. Chem. B. 5 (2017) 6681–6687. doi:10.1039/C7TB01557G.

[35] T. Pirmohamed, J.M. Dowding, S. Singh, B. Wasserman, E. Heckert, A.S. Karakoti, J.E.S. King, S. Seal, W.T. Self, Nanoceria exhibit redox state-dependent catalase mimetic activity, Chem. Commun. 46 (2010) 2736–2738. doi:10.1039/b922024k.

[36] Z.N. De Pourbaix M, Atlas of Electrochemical Equilibria in Aqueous Solutions, National Association of Corrosion Engineers, Houston, 1974.

[37] K. Reed, A. Cormack, A. Kulkarni, M. Mayton, D. Sayle, F. Klaessig, B. Stadler, Exploring the properties and applications of nanoceria: is there still plenty of room at the bottom?, Environ. Sci. Nano. 1 (2014) 390–405. doi:10.1039/C4EN00079J.

[38] S.M. Hirst, A. Karakoti, S. Singh, W. Self, R. Tyler, S. Seal, C.M. Reilly, Bio-distribution and in vivo antioxidant effects of cerium oxide nanoparticles in mice., Environ. Toxicol. 28 (2013) 107–18. doi:10.1002/tox.20704.

[39] A.B. Shcherbakov, N.M. Zholobak, A.E. Baranchikov, A. V Ryabova, V.K. Ivanov, Cerium fluoride nanoparticles protect cells against oxidative stress, Mater. Sci. Eng. C. 50 (2015) 151–159. doi:https://doi.org/10.1016/j.msec.2015.01.094.

[40] X. Jiao, H. Song, H. Zhao, W. Bai, L. Zhang, Y. Lv, Well-redispersed ceria nanoparticles: Promising peroxidase mimetics for H2O2 and glucose detection, Anal. Methods. 4 (2012) 3261–3267. doi:10.1039/C2AY25511A.

[41] W. Zhang, G. Xie, S. Li, L. Lu, B. Liu, Au/CeO2–chitosan composite film for hydrogen peroxide sensing, Appl. Surf. Sci. 258 (2012) 8222–8227. doi:https://doi.org/10.1016/j.apsusc.2012.05.025.

[42] L. Gao, J. Zhuang, L. Nie, J. Zhang, Y. Zhang, N. Gu, T. Wang, J. Feng, D. Yang, S. Perrett, X. Yan, Intrinsic peroxidase-like activity of ferromagnetic nanoparticles., Nat. Nanotechnol. 2 (2007) 577–83. doi:10.1038/nnano.2007.260.

[43] F. Qiao, J. Wang, S. Ai, L. Li, As a new peroxidase mimetics: The synthesis of selenium doped graphitic carbon nitride nanosheets and applications on colorimetric detection of H2O2 and xanthine, Sensors Actuators B Chem. 216 (2015) 418–427. doi:https://doi.org/10.1016/j.snb.2015.04.074.

[44] H. Zhao, Y. Dong, P. Jiang, G. Wang, J. Zhang, Highly Dispersed CeO2 on TiO2 Nanotube: A Synergistic Nanocomposite with Superior Peroxidase-Like Activity, ACS Appl. Mater. Interfaces. 7 (2015) 6451–6461. doi:10.1021/acsami.5b00023.

[45] X. Wang, W. Cao, L. Qin, T. Lin, W. Chen, S. Lin, J. Yao, X. Zhao, M. Zhou, C. Hang, H. Wei, Boosting the peroxidase-like activity of nanostructured nickel by inducing its 3+ oxidation state in LaNiO3perovskite and its application for biomedical assays, Theranostics. 7 (2017) 2277–2286. doi:10.7150/thno.19257.

[46] J. Li, J. Wen, B. Li, W. Li, W. Qiao, J. Shen, W. Jin, X. Jiang, K.W.K. Yeung, P.K. Chu, Valence State Manipulation of Cerium Oxide Nanoparticles on a Titanium Surface for Modulating Cell Fate and Bone Formation, Adv. Sci. 5 (2018) 1700678–15. doi:10.1002/advs.201700678.